Vacuum 218 (2023) 112596

Contents lists available at ScienceDirect

Vacuum

journal homepage: www.elsevier.com/locate/vacuum

Improvement of the piezoelectric response of AlN thin films through the evaluation of the contact surface potential by piezoresponse force microscopy

M.A. Signore [a,*], L. Francioso [a], C. De Pascali [a], A. Serra [b], D. Manno [b], G. Rescio [a], F. Quaranta [a], E. Melissano [a], L. Velardi [a]

[a] Institute for Microelectronics and Microsystems, CNR-IMM of Lecce, 73100, Lecce, Italy
[b] University of Salento, Department of Mathematics and Physics, 73100, Lecce, Italy

ARTICLE INFO

Handling Editor: Prof. L.G. Hultman

Keywords:
Aluminum nitride
RF magnetron sputtering
Piezoelectric response
Piezoresponse force microscopy (PFM)
Kelvin probe force microscopy (KPFM)
Surface potential

ABSTRACT

Sputtered aluminum nitride (AlN) thin films were characterized by Piezoresponse Force Microscopy (PFM) technique using a methodology to decrease the contribution of the electrostatic forces to obtain a pure piezoelectric response. Our method is based on the sweeping of the DC voltage applied to the Atomic Force Microscope (AFM) tip under a fixed AC field to evaluate the contact surface potential difference (V_{CPD}) between the tip and the sample used to measure the proper AlN piezoelectric coefficient ($d_{33,eff}$), minimizing the electrostatic contribution. Kelvin probe Force Microscopy (KPFM) was employed as reference standard technique to measure the surface potential, confirming the reliability of the proposed experimental procedure on ceramic piezoelectric films, and simultaneously overcoming the disadvantages of the KPFM technique. The capability to tune surface potential of materials over a wide range of values opens new perspectives for the design of devices with changeable surface potential.

1. Introduction

Atomic Force Microscopy (AFM) is a cutting-edge tool for surface characterization of organic and inorganic materials at microscale and nanoscale levels [1,2]. This technique has been extended by the combination with other surface characterization techniques which allow the access to further information with high spatial resolution. Two representatives of these enhanced AFM techniques are Piezoresponse Force Microscopy (PFM) [3] and Kelvin Probe Force Microscopy (KPFM) [4,5].

PFM is a contact technique used to measure out-of-plane electromechanical deformation of a material resulting from an applied out-of-plane electric field to the sample through the AFM tip, providing information about piezoelectric properties of the materials. Since the electric field induces a strain, this is referred to as the converse piezoelectric effect [6]. KPFM is a noncontact technique which provides a spatially resolved measurement of the electrostatic force between the AFM tip and the sample under test. Both techniques provide an understanding of the correlation between polarization and screening charges in the analysed materials.

During PFM measurement, AFM generally operates in contact mode being the cantilever continuously in contact with the sample at a constant force. The sample is mounted on a conductive substrate and an AC electrical field (V_{AC}) is applied over the sample through a conductive tip used as second electrode. The AC drive voltage applied between the tip and the investigated material causes a periodic expansion and/or contraction of the sample. This oscillatory movement of the sample surface induces a periodic cantilever bending that is analysed by the AFM controller's lock-in amplifier. The PFM imaging provides the amplitude and phase response of the cantilever and, simultaneously, the surface topography. The amplitude gives information about the magnitude of the deformation while phase contrast shows the direction of the electrical polarization relative to electrical field. These parameters allow for the evaluation of the effective piezoelectric coefficient $d_{33,eff}$. With a purely out-of-plane response, the most common way to evaluate the piezoresponse of a material is to sweep the applied AC field over the sample and to plot the corresponding measured amplitude (A) of the oscillation. The slope of the linear regression provides the effective piezoelectric coefficient $d_{33,eff}$. The linear fit generally does not cross the

* Corresponding author.
E-mail address: mariaassunta.signore@cnr.it (M.A. Signore).

https://doi.org/10.1016/j.vacuum.2023.112596
Received 27 June 2023; Received in revised form 8 September 2023; Accepted 8 September 2023
Available online 9 September 2023

origin of the graph due to other additional contributions to the signal affecting the piezoelectric response such as material clamping, inhomogeneous field effects, electrochemical strain (due to electrochemical reactions and ionic motion), Joule heating (if the material is conductive) and electrostatic effects (when the tip is in contact with the sample surface) [7,8]. Electrostatic contribution always occurs, and it is due to the presence of a potential difference between the AFM tip/cantilever and the sample surface (i.e. the surface potential). This potential is attributed to the electrostatic force induced by the Coulomb interaction between separated charges of AFM tip/cantilever and of the sample surface. Due to the intrinsic nature of the surface potential, this is the most important non-piezoelectric contribution that occurs during PFM measurements [9]. In fact, it increases or decreases the PFM amplitude (depending on the relative signs between the surface potential and the external DC voltage, V_{DC} [10]), modifies the phase images and distorts the shape of the PFM hysteresis loop [11].

The tip response R_{tip} can be described by the following formula [12]:

$$R_{tip} = d_{eff} V_{AC} + k_c^{-1} \times \frac{\partial c}{\partial z} \times V_{AC}[V_{DC} - V_{CPD}] = R_1 + R_2 \quad (1)$$

where k_c is the contact stiffness of the cantilever and V_{CPD} is the contact potential difference between tip and sample. Tip response can be split into two different components, as reported in (1), i.e. R_1 and R_2. R_1 represents the piezoelectric response simply obtained by V_{AC} sweeping and by calculating the slope of the linear regression of the film displacement against electric field, R_2 takes into account the electrostatic interaction between sample and tip. It can be clearly deduced that the conventional AC signal sweeping does not compensate for the electrostatic contribution expressed by R_2, so that the value of the piezoelectric coefficient d_{33} is higher than it is actually. To account for the electrostatic effect expressed by R_2 and for a more accurate evaluation of this component, two strategies can be followed: (1) to use a high stiffness k_c cantilever; (2) to evaluate the V_{DC} point value such to minimize the electrostatic response ($V_{DC} = V_{CPD}$). The use of high stiffness AFM cantilever is a well consolidated strategy to lower electrostatic component of ceramic-based piezoelectric materials but does not eliminate it [7]. On the contrary, no attempt to follow the second strategy for ceramic materials have never been discussed in literature to our best knowledge. In the work of Miller et al. [13] an approach is proposed to evaluate V_{DC} point for soft organic materials, by exploiting the possibility, during PFM measurement, to add a DC bias voltage to the tip so that the potential applied to the sample is $V_{AC} + V_{DC}$. As a matter of fact, the second strategy implies the knowledge of the local contact potential difference V_{CPD}. Therefore, it is crucial to know the influence of electrostatic interaction (i.e. the surface potential) on the PFM signal to derive the correct piezoelectric coefficient value for the material under examination.

KPFM is the technique used to perform nanoscale imaging of surface potential i.e. V_{CPD} for a variety of materials [14,15]. This potential is related to the difference between tip and sample work functions when the sample is a metal. During KPFM measurement, AFM tip approaches to the sample without contact, and an electrical force is generated between the tip and sample surface, due to the differences in their Fermi energy levels. The equilibrium requires Fermi levels alignment through electrons current flow. Both sample and tip will be charged and contact potential difference will be generated causing the presence of an electrical force at the contact area. V_{CPD} is evaluated from the change in the resonance frequency or amplitude of the cantilever by applying an AC bias voltage which modulates the electrostatic interaction force between the tip and the sample. This force can be eliminated by applying an external bias of the same magnitude and opposite direction on the tip. In other words, KPFM provides the values of the surface potentials (V_{CPD}) that minimizes the electrostatic force between tip and samples by applying a V_{DC} which corresponds to V_{CPD} and consequently to the work functions difference between tip and analysed film [16].

Nevertheless, KPFM has some disadvantages in measuring the surface potential or work function of a sample [17]. First, the KPFM measure requires to know the work function of the probe or the calibration of KPFM probe on a standard sample (with a well-defined work function). Therefore, two measurements are needed, one on the reference surface and one on the sample and it decreases the accuracy of the measurement. Second, the change of the distance between tip and sample during the measurement modifies the capacitance gradient i.e. the electrical force between the tip and sample. Consequently, the measured surface potential value does not represent V_{CPD}. Finally, KPFM works better on metals than on semiconductor, especially doped semiconductor [18] because of work function variations due to defect states.

In addition to be a valid support for reliable piezoelectric measurements, the evaluation of the surface potential and of its variations over a solid surface or solid-liquid interface at sub-nanometer resolution is of great interest also in many other fields of application and processes [19,20]. Changes in the electrostatic potential are extremely crucial for the interpretation, prediction and engineerization of the response of potentiometric biosensing platforms such as ion-sensitive field-effect transistors (IS-FETs) and field-effect biosensors (BioFETs) [21]. In addition, several variables that induce potential change. i.e. adsorption of target molecules [22,23], biological species [24], bacteria adhesion and ageing [25–27], catalysis and photocatalysis [28], nanoparticle separation [29] can be detected through surface potential measurement, being a significant surface property for cell-matrix interfaces and tissue engineering [30]. Recent literature reports surface potential tuning as a promising strategy to reprogram the immune microenvironment for bone regeneration, providing solid bases for the development of biomaterials with immunomodulatory functions [31]. It has been observed that a surface potential of 391 mV on Ti surface was the most favourable for the osteogenic differentiation of MC3T3-E1, which was closely related to the binding state of the adsorbed fibronectin [32]: this opens the possibility to design implants with changeable surface potential by connecting biomaterials to a power source or coupling with external fields. To this aim, biocompatible piezoelectric materials, like aluminum nitride (AlN) thin films, merit a special attention thanks to their capability to generate charges on surface (or surface potential) when stretched, and vice versa, allowing for a precise control of cells allocation and proliferation [33,34]. In this paper, two AlN samples grown by RF magnetron sputtering technique at different substrate temperature, i.e. room temperature (AlN_RT) and 150 °C (AlN_150), have been compared in terms of piezoelectric performance. The effect of the electrostatic component on the piezoelectric response of AlN thin films is investigated, and a way to minimize it for obtaining an electrostatic-free PFM signal is demonstrated, by exploiting only conventional PFM measurements. In addition to conventional method for $d_{33,eff}$ evaluation and the use of high-k_c cantilever for the minimization of electrostatic effect, another strategy was proposed. Specifically, a sweep of DC voltage (V_{DC}) at different fixed AC signals (V_{AC}) was applied to the samples, with the aim to estimate the contact surface potential such to minimize the electrostatic contribution on the AlN piezoelectric response. KPFM was employed as gold standard technique to evaluate the surface potential of the analysed films at a fixed AC amplitude to confirm the reliability of the proposed experimental procedure. The results obtained by the two techniques have resulted comparable, confirming the consistency of the alternative method for surface potential calculation of ceramic piezoelectric films.

2. Experimental details

AlN thin films were deposited by RF magnetron sputtering on Low Resistivity silicon (LR-Si) substrate by using a 99.999 % pure Al target, in pure Ar and N_2 gas mixture, which were introduced into the chamber by separate mass flow controllers. The base pressure of the sputtering chamber was 2.5×10^{-7} mbar before depositions. For all the depositions, the N_2 flux percentage in the reactive mixture was fixed at 60

%, the RF power applied to Al target at 150 W and the total pressure at 4 × 10^{-3} mbar. Two different films 500 nm-thick were characterized by changing only the substrate temperature and keeping constant the sputtering atmosphere conditions. The temperature values were room temperature (the sample was labelled as AlN_RT) and 150 °C (labelled AlN_150), known as a sputtering parameter generally tuned to improve the (002) wurtzite arrangement and, as consequence, the piezoelectric response of the thin films. Both samples were deposited on a 150 nm-thick Ti seed layer, sputtered at room temperature on Si substrate in Ar atmosphere at a process pressure equal to 2.5 × 10^{-2} mbar. The target-substrate distance was fixed to 80 mm.

The crystalline structure and orientation of AlN films were analysed by X-ray diffraction by using the Cu-Kα radiation and scanning angle of 2θ = 10–80°. The spectra curves were fitted by a Voigt function to extract the full width at half maximum (FWHM) for crystal quality assessment.

The surface topography, morphology, and roughness of the AlN films were investigated by Atomic Force Microscopy (AFM) analyses. AFM topography 2D and 3D images were acquired over 1 μm × 1 μm scan areas (resolution of 256 × 256 points) by a Nanosurf CoreAFM instruments operating in non-contact mode, at room temperature and in air environment. Silicon probe tips with Diamond-Like-Carbon conductive coating (MULTI75-DLC) were used at the typical resonance frequency of 75 kHz, with a constant force of 3 N/m.

Piezoelectric response on the nanoscale was investigated by PFM analysis by scanning 0.5 μm × 0.5 μm areas at five different positions on the films surface, for both samples. Two cantilevers with different stiffness, i.e. low-k_c- MULTI75-DLC (k_c = 3 N/m) and high-k_c-TAP300E-G (k_c = 40 N/m) were used. For this purpose, a sweep of AC driving amplitude (V_{AC}) in the range 2–5 V was applied to the tip at frequency of 3 kHz, well below the used cantilevers contact resonance (MULTI75-DLC has a resonance frequency of 75 kHz and TAP300E-G of 300 kHz [35]) to prevent the crosstalk between the signals of the topography and the piezoelectric response recorded simultaneously. Amplitude and phase of the PFM signal provide information about the local piezoelectric deformation along *z*-direction and the individual grain polarity, respectively. By using the low-k_c cantilever (MULTI75-DLC), PFM analysis was performed for the calculation of the contact surface potential V_{CPD} by sweeping V_{DC} (−3 V–3 V) at fixed V_{AC} (in the range 2–5 V).

KPFM technique was employed to compare the measurements with the experimental results of the proposed method. As with PFM analyses, 0.5 μm × 0.5 μm areas were analysed for both samples at five different positions on the surface of the films. During KPFM measurement, an AC voltage amplitude V_{AC} = 2 V and a frequency of 17 kHz were applied to a MULTI75E-G cantilever with Cr/Pt-coated tip. Before to measure the samples, the work function of the probe was calibrated by using a sample test with Al and Au line arrays, and the work function of the tip was evaluated. The measured contact potential difference (V_{CPD}) is the potential difference between the sample and the tip as expressed by $V_{CPD} = (\varphi_{sample} - \varphi_{tip})/e$ where φ_{tip} and φ_{sample} are the work functions of the tip and sample, respectively, and e is the elementary charge. During the scan, the tip is positioned very close (a few tens of nm at most) to the analysed sample. By modulating the bias voltage, the electrostatic force between tip and the thin film is nullified by a controller, thus giving out the local surface potential, which describes the charge distribution (i.e. surface potential) on the sample surface.

3. Results and discussion

3.1. Structural and morphological properties of AlN thin films deposited at different substrate temperature

XRD analysis was performed to verify the structural arrangement of AlN planes of wurtzite along (002) direction, which guarantees a piezoelectric response. Fig. 1 shows XRD spectra of both analysed samples, according to their deposition temperature.

Both AlN films exhibit a (002)-high orientation together with reflections coming from Ti seed layer. While AlN_RT sample diffractogram shows two reflections from Ti film, attributable to Ti (100) and Ti (002) of exagonal structure, only (002)-oriented crystallites are observed in the AlN_150 spectrum. This structural modification is due to the higher

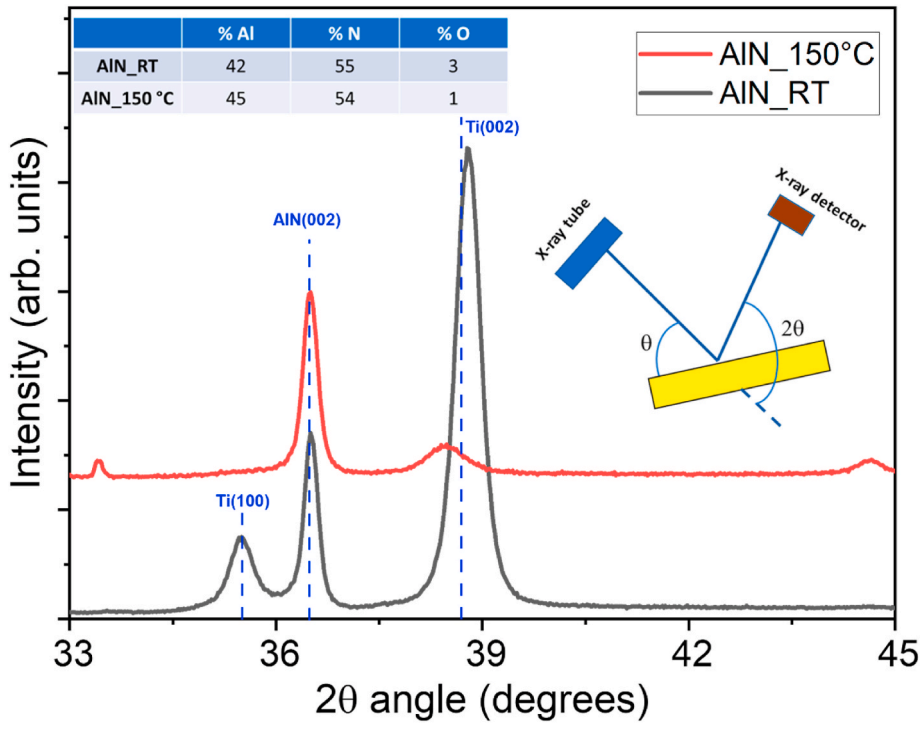

Fig. 1. XRD spectra of AlN films deposited at deposition temperature equal to RT (black line) and 150 °C (red line). In the table of the inset the stoichiometry compositions of the films obtained by RBS spectra analysis using SIMNRA software are reported.

deposition temperature. Before AlN deposition, the Si substrate covered with Ti seed layer is positioned into the deposition chamber on the substrate holder that is heated up to 150 °C in vacuum of 5×10^{-7} mbar. This moderate annealing process causes a peak shift of Ti (002) reflection towards lower 2θ angle indicating the generation of compressive stress into the lattice during heating process [36]. At the same time, heating step promotes crystal lattice modifications, with a structural switch of (100)-oriented grains into (002)-oriented ones, resulting from the competition between strain energy and surface free energy affecting the textures of the grains [37]. They result smaller (25.8 nm) than Ti (002)-oriented grains of the AlN_RT film (29.3 nm), as evaluated by Debye-Scherrer formula by considering the parameters obtained through Voigt fitting of XRD curves [38]. This preferential orientation along (002) planes promotes a better structural arrangement of the AlN thin film, as already observed. By following the same fitting procedure, the AlN (002)-grain size has been calculated too. The film deposited at higher temperature shows a better structural arrangement with an improved grain size equal to 45.9 nm compared to 39.7 nm of the film deposited at room temperature. This finding is also supported by the lowering of oxygen contaminant incorporation with temperature increasing [39], as confirmed by Rutherford Backscattering Spectrometry (RBS) measurements performed by the CEDAD-Centre of Applied Physics, Dating and Diagnostics (University of Salento) using a 3 MV Tandetron accelerator [40]. The acquired spectra were analysed by SIMNRA software which provides the stoichiometric composition of the films reported in the table of the inset in Fig. 1.

Fig. 2 reports the 2D and 3D AFM images of the AlN thin films. Different surface topographies are evident: the AlN_RT image (Fig. 2a) shows a less compact structure and grain aggregates which correspond to a higher surface roughness R_q (as reported in the Figure) while AlN_150 exhibits a denser and smoother grain arrangement (Fig. 2b). This is a direct consequence of the different deposition temperature. Once again, a higher temperature induces a better texture degree of the film, favouring the columnar structure normal to the substrate as also a higher adatoms mobility which promotes less rough surface formation. These results are in accordance with XRD analyses.

3.2. *Piezoelectric characterization of AlN thin films: two approaches to minimize the influence of the electrostatic component on the piezoelectric response*

The structural arrangement of the AlN thin films along (002)-planes of the hexagonal wurtzite guarantees a piezoelectric response whose intensity depends on the degree of *c*-axis orientation which is strictly correlated to the deposition parameters. The piezoresponse of the AlN samples was initially determined considering standard method, i.e. by sweeping the AC electric field (V_{AC}) applied to the tip and plotting the corresponding amplitude value against it. Two different tips were used, according to their stiffness coefficient k_c: TAP300E-G ($k_c = 40$ N/m) and MULTI75-DLC ($k_c = 3$ N/m). The slope of the linear fit provides the effective $d_{33,eff}$. This first approach was followed to verify the influence of the cantilever stiffness on the minimization of the electrostatic influence on samples piezoelectric response, according to formula (1). Fig. 3 depicts the thin films displacement versus V_{AC} for AlN_RT thin film by using low-k_c (Fig. 3a) and high-k_c (Fig. 3b) cantilever, respectively. Fig. 3c shows representative PFM images (topography/amplitude/phase) obtained with MULTI75-DLC cantilever, at V_{AC} equal to 2 V.

In the same way, Fig. 4 summarizes the results for the AlN sample deposited by heating the substrate up to 150 °C.

Figs. 3 and 4 provide a lot of information. As expected, the AlN film deposited at higher temperature shows a better piezoelectric response (see Fig. 3a and 4a), confirming the structural and morphological results provided by XRD and AFM analyses. The piezoelectric behaviour of the two films is clearly evident in the PFM amplitude images and the corresponding horizontal profiles (Fig. 3c and 4c): the magnitude of the vertical deformation expressed in μV (amplitude images) is greater for the AlN_150 sample, resulting in a higher $d_{33,eff}$ value. Moreover, the AlN_150 sample shows also better polarization directions (phase images), with more grains with 180° phase direction (see horizontal phase profiles), because of the better structural arrangement of the film growth at higher temperature.

Moreover, the $d_{33,eff}$ values obtained by using a low-k_c tip for PFM measurements are higher than those calculated by fitting experimental data coming from high-k_c tip scans [41]. It decreases from −3.71 pm/V to −2.65pm/V for AlN_RT film, and from −4.44 pm/V to −3.77 pm/V

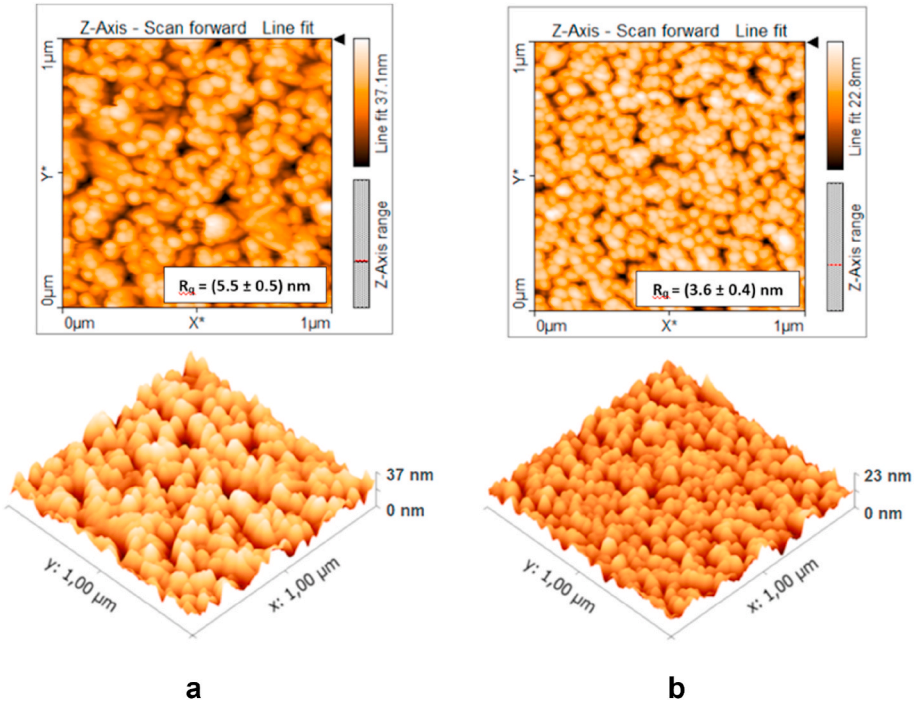

Fig. 2. 2D (up) and 3D (down) AFM images of AlN films deposited at deposition temperature equal to (a) RT and (b) 150 °C.

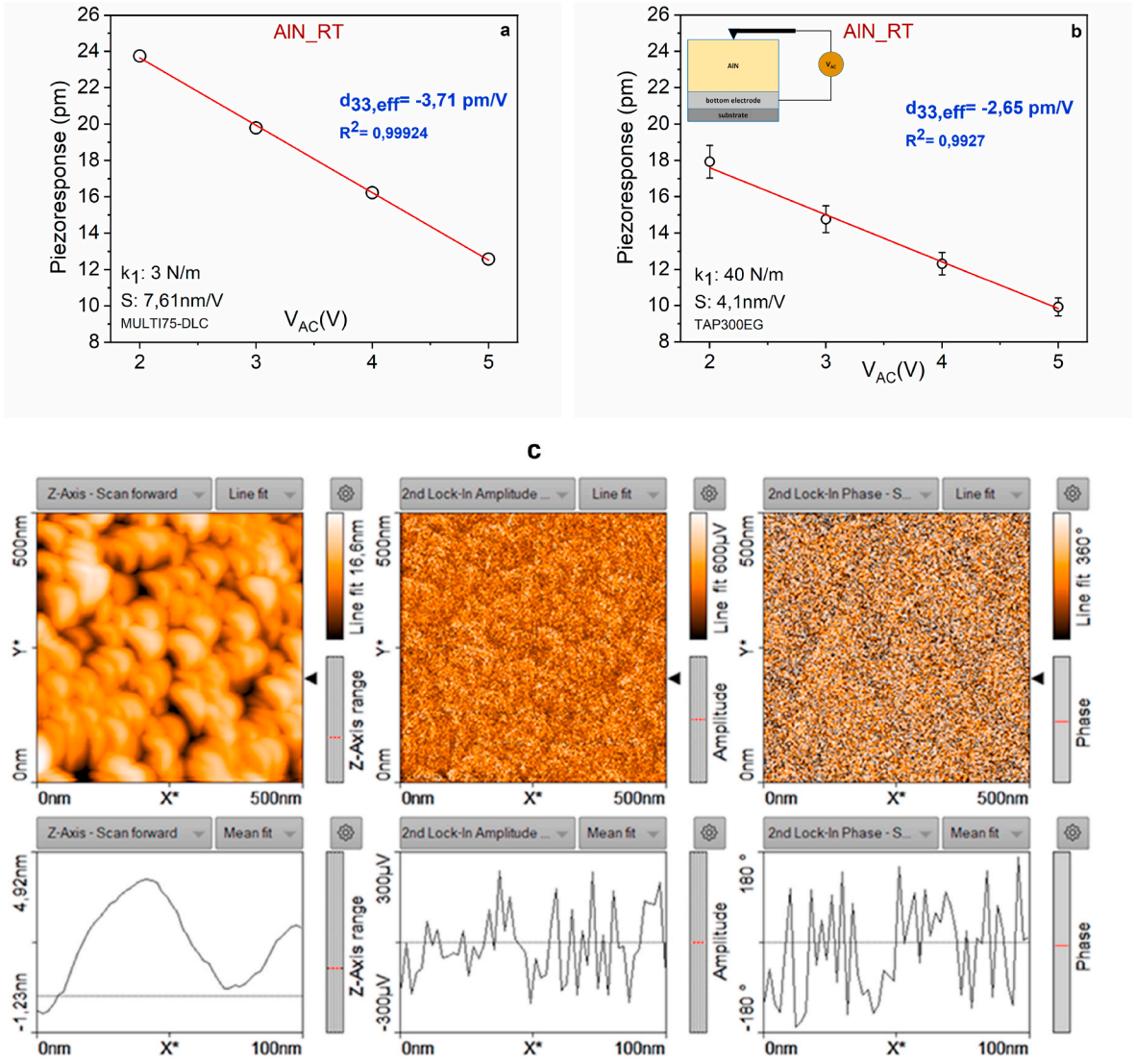

Fig. 3. Comparison between $d_{33,eff}$ values of the analysed AlN thin films deposited at RT, according to the tip stiffness (a–b); PFM topography/amplitude/phase image obtained at V_{AC} = 2 V within the corresponding horizontal profiles related to a scan-line of 100 nm (c).

for AlN_150 film, by increasing cantilever stiffness. The negative piezoelectric coefficient values suggests that the polarity of both films is predominantly oriented opposite to the substrate (N-polar) [42]. The results reported in Figs. 3b and 4b confirm that the use of a high-k_c PFM tip is a valid attempt to reduce electrostatic contribution for ceramic-based piezoelectric materials, as deducible from the second term of formula (1). The same term suggests another way to minimize this contribution, never employed for ceramic thin films. It requires to know the contact surface potential generated when AFM tip is in contact with the scanned sample. In this work, the contact surface potential was calculated by following the work of Miller et al. [12] where the method was applied to soft materials. AFM was used in contact mode to account for the electrostatic component, and a sweep of DC signal (V_{DC}) was considered for both analysed samples during the standard measurement for $d_{33,eff}$ calculation. V_{DC} was tuned in the range (−3 V ÷ 3 V) for each AC signal (V_{AC}). The V_{DC} point at which the electrostatic response is minimized is evaluated for each considered V_{AC} (Figs. 3a and 4a). Figs. 5 and 6 show the plots of experimental data obtained by employing the above-described procedure for the AlN thin films deposited at RT and 150 °C, respectively. The trend of the contact surface potential versus AC signal is plotted, too (Fig. 5b and 6b).

The surface potential values vary in different range according to the deposition temperature of the analysed film. Specifically, they vary from 108 to 352 mV by increasing the alternate signal V_{AC} from 2 to 5 V for AlN_RT thin film, and from 112 to 252 mV in the same AC signal range for the film deposited at 150 °C. In both cases, it is evident the linear trend versus AC signal followed by V_{CPD} which increases with AC signal. The difference of the contact surface potentials of the two samples at the same values of voltage signals is probably due to different surface properties (i.e. chemistry, surface state, surface charge, impurity concentration [43]), related to different deposition conditions, which have the main influence on surface potentials. This procedure should help to make more accurate the traditional AC sweep method for the calculation of the piezoelectric coefficients. For this reason, the measurements shown in Fig. 3a (AlN_RT) and 4a (AlN_150) were performed again by applying an additional V_{DC} signal to the V_{AC} one applied to the tip, exactly equal to the evaluated contact surface potential for each AC voltage (Figs. 5 and 6). This step is aimed to eliminate (or minimize) the electrostatic term of equation (1). As a matter of fact, when the applied V_{DC} is exactly equal to V_{CPD} value, electrostatic component should be nullified, leaving active only the piezoelectric contribution of the material when excited by the electric field. The results obtained by following this procedure are shown in Fig. 7a and b for the samples deposited at RT and higher temperature, respectively.

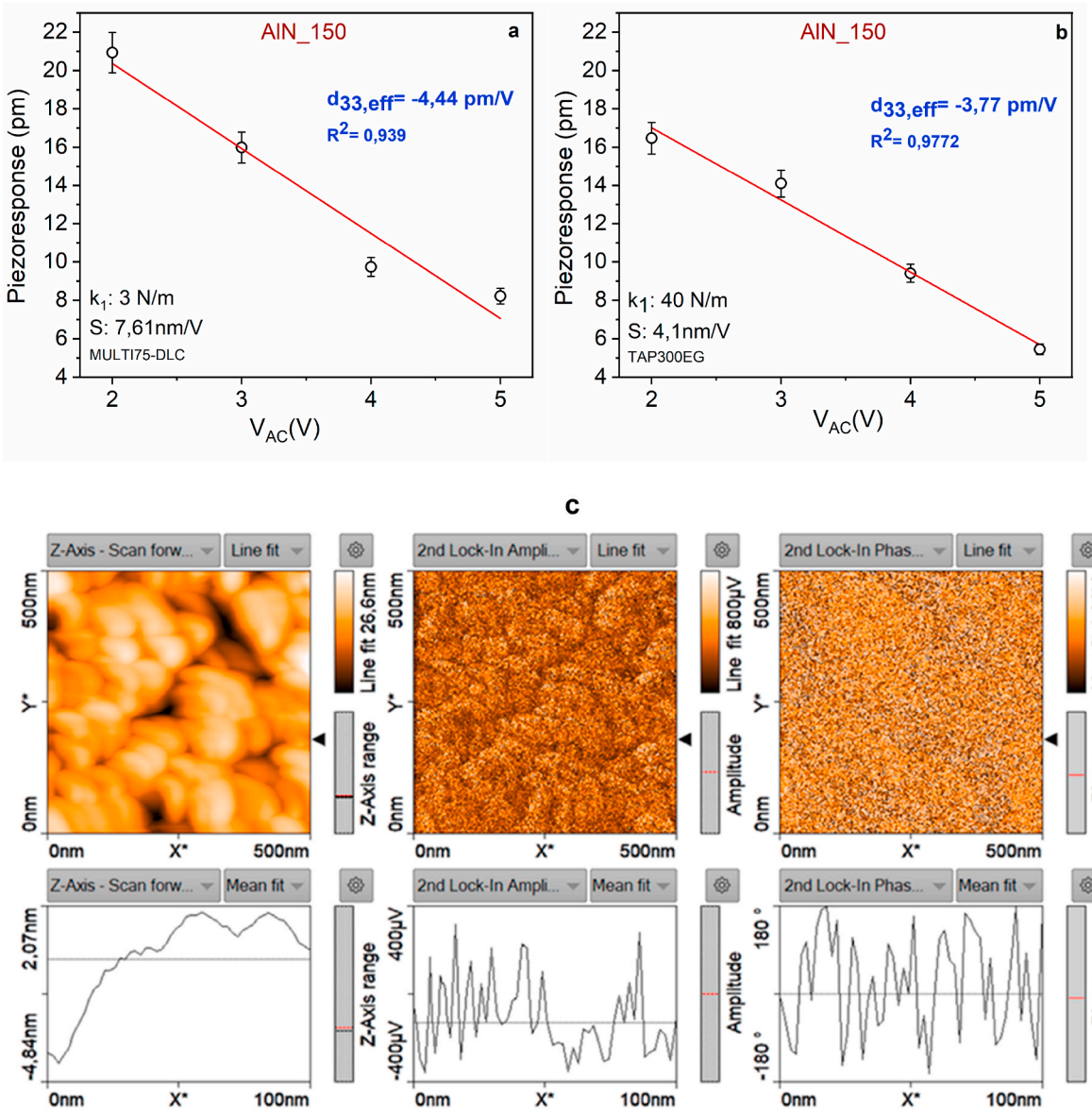

Fig. 4. Comparison between $d_{33,eff}$ values of the analysed AlN thin films deposited at substrate temperature equal to 150 °C, according to the tip stiffness (a-b); PFM topography/amplitude/phase image obtained at V_{AC} = 2 V within the corresponding horizontal profiles related to a scan-line of 100 nm (c).

The results demonstrate that this method provides a lower $d_{33,eff}$ when the additional DC potential is applied to the tip, contributing to the minimization/elimination of the electrostatic extra component to the output piezo-response. The piezoelectric coefficient decreases from −3.71 pm/V to −2.36 pm/V for AlN_RT thin film, and from −4.44 pm/V to −3.35 pm/V for the high temperature-deposited one. Moreover, it is very interesting to note that the values obtained with the last procedure were also lower than those obtained by using the TAP300E-G cantilever. This confirms that the use of a high elastic constant cantilever reduces the contribution of the electrostatic force, but it results less effective than the discussed methodology using the surface potential. Table 1 reports a summary of the $d_{33,eff}$ values obtained using the different approaches discussed in the paper. by different methodologies.

Moreover, it is evident from Table 1 the greater electrostatic contribution on the $d_{33,eff}$ coefficient of AlN_RT sample with respect AlN_150. As already mentioned, the electrostatic interaction between the AFM tip/cantilever and the sample modifies the PFM signals and depends on the material and tip properties. Generally, in PFM measurements performed under the same experimental conditions (same material, cantilever type, applied voltages), the contribution of electrostatic interaction becomes more significant in less piezoelectric materials, while its impact is less intense in samples with a higher $d_{33,eff}$ coefficient.

Finally, starting from the values obtained with electrostatic contribution correction, a further improvement in the piezoelectric coefficient calculation can be performed by considering the clamping effect of the substrate on the thin film which restrains the sample volume change. A known relation allows for the calculation of the unclamped d_{33} by using the clamp effect correction factor C_{clamp} equal to 1.4 for AlN thin films [44]. Considering the correction, the piezoelectric coefficient of the AlN_RT thin film is −3.30 pm/V and for AlN_150 is equal to −4.69 pm/V. Our results are in good agreement with literature ones where, for AlN thin films (002)-oriented, the reported $d_{33,eff}$ values belong to the range of 2.5–6.8 pm/V without any correction procedure to nullify electrostatic influence [45,46].

4. Validation of the methodology: KPFM measurements

To validate this procedure, KPFM measurements were performed on both samples. Generally, this measure is performed at fixed tip voltage

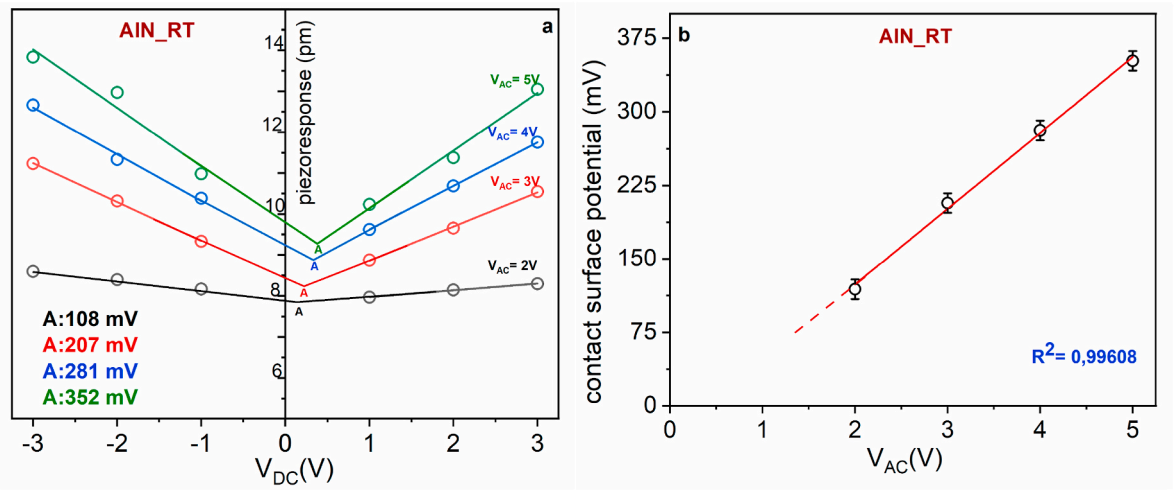

Fig. 5. Piezoresponse of RT deposited-AlN thin film by sweeping V_{DC} voltages at fixed V_{AC} applied to the AFM tip (a); contact surface potential values obtained at each fixed V_{AC} applied to the tip, obtained from the intersection between the linear fit curves of positive and negative DC voltages (b).

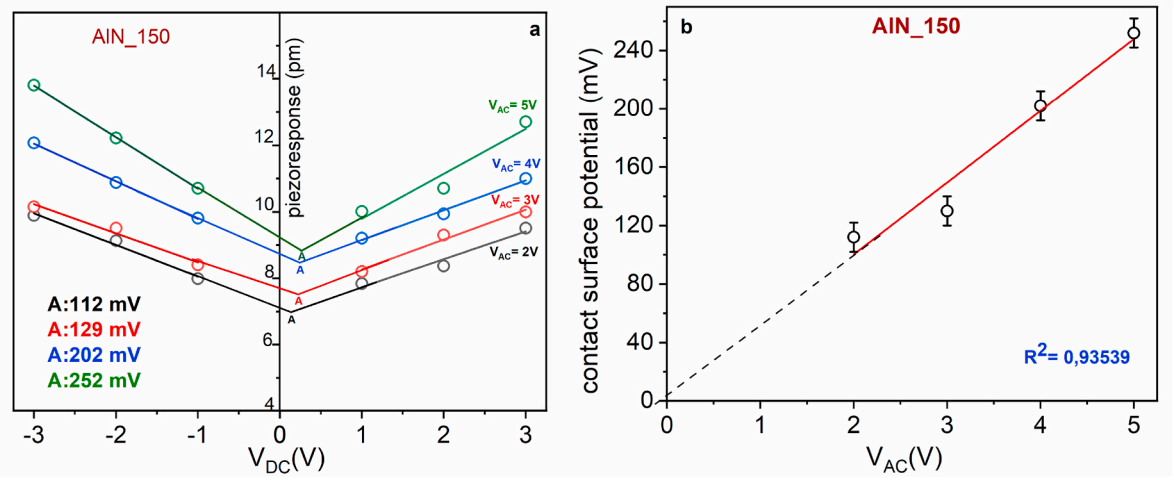

Fig. 6. Piezoresponse of 150 °C deposited-AlN thin film by sweeping V_{DC} voltages at fixed V_{AC} applied to the AFM tip (a); contact surface potential values obtained at each fixed V_{AC} applied to the tip, obtained from the intersection between the linear fit curves of positive and negative DC voltages (b).

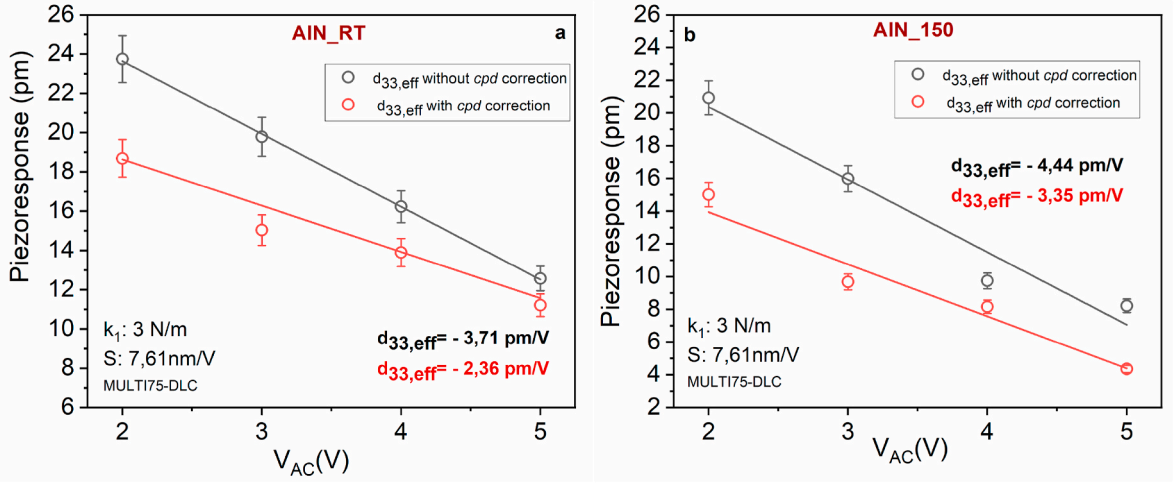

Fig. 7. Piezoelectric coefficient evaluated after the application of an additional DC voltage to AFM tip equal to the surface contact potential calculated at fixed AC signal, for AlN deposited at RT (a) and at 150 °C (b).

Table 1
Piezoelectric coefficient values (d33, eff) obtained by different methodologies.

Sample	$d_{33,eff}$ (pm/V)			
	MULTI75-DLC (k_c = 3 N/m)	TAP300E-G (k_c = 40 N/m)	by calculating V_{CPD} with low-k cantilever	Electrostatic contribution on $d_{33/eff}$ value (absolute value)
AlN_RT	- 3.7 ± 0.2	- 2.7 ± 0.4	**- 2.4 ± 0.3**	**1.4**
AlN-150	- 4.4 ± 0.7	- 3.8 ± 0.5	**- 3.4 ± 0.5**	**1.1**

V_{AC} which should be accurately selected, together with other important parameters, to have a stable, repeatable, and reliable measurement. Two of the most important parameters to choose to obtain highly resolute and reliable measurements are (1) the working frequency for the electrostatic excitation, which is the frequency related to V_{AC} well below the mechanical resonance of the probe, and (2) the cantilever. The smallest detectable signal of V_{CPD} by KPFM technique can be expressed by the following formula:

$$V_{CPD,min} = \frac{d}{\varepsilon_0 V_{AC} R}\sqrt{\frac{2 k_B T k_c B}{\pi^3 Q f_0}} \quad (2)$$

where the R is the tip radius, d is the tip-sample distance, T is the temperature, k_c is the cantilever spring constant, Q is the quality factor, B is the bandwidth, f_0 is the resonance frequency of the cantilever, k_B is the Boltzmann constant, V_{AC} is the amplitude of the AC voltage between the tip and the sample and the ϵ_0 is the dielectric constant of vacuum.

The formula provides some indications about the most favourable requisites to obtain high resolution measurements. Softer and shorter cantilever with larger tip radius is beneficial for KPFM sensitivity (k_c = 3 N/m and R = 25 nm for MULTI75E-G), as well a specific AC amplitude for a better signal-to-noise ratio (SNR). According to (2), a wide V_{AC} should be favourable but too large AC amplitudes cause a reduction in the lateral resolution which makes rougher the curves recorded by KPFM scans, while a low V_{AC} makes the measurement inaccurate, resulting in incorrect surface potential values. For this reason, the check of the best AC amplitude should be done before performing the final analysis, to guarantee the best measurement. Similarly, this check allows for setting tip voltage modulation amplitude to a value corresponding to the highest force response. The force response is proportional to the modulation amplitude, so large amplitude will give a larger response.

In our experimental conditions, related also to the analysed material, the best AC amplitude value for the highest lateral resolution resulted to be 2 V. Thus, KPFM measurement was performed on both samples at this V_{AC}, at which the surface potential response was most stable and repeatable and, at the same time, most intense.

Fig. 8 shows the images obtained by KPFM analysis for the AlN_RT (a) and AlN_150 (b) samples.

The two images show a good KPFM contrast thanks to the high spatial resolution of the measures. The voltage maps (area of 500 × 500 nm^2) within the horizontal tip voltage profiles (250 nm of scan length) in Fig. 8 show a higher surface potential for the AlN_150 sample.

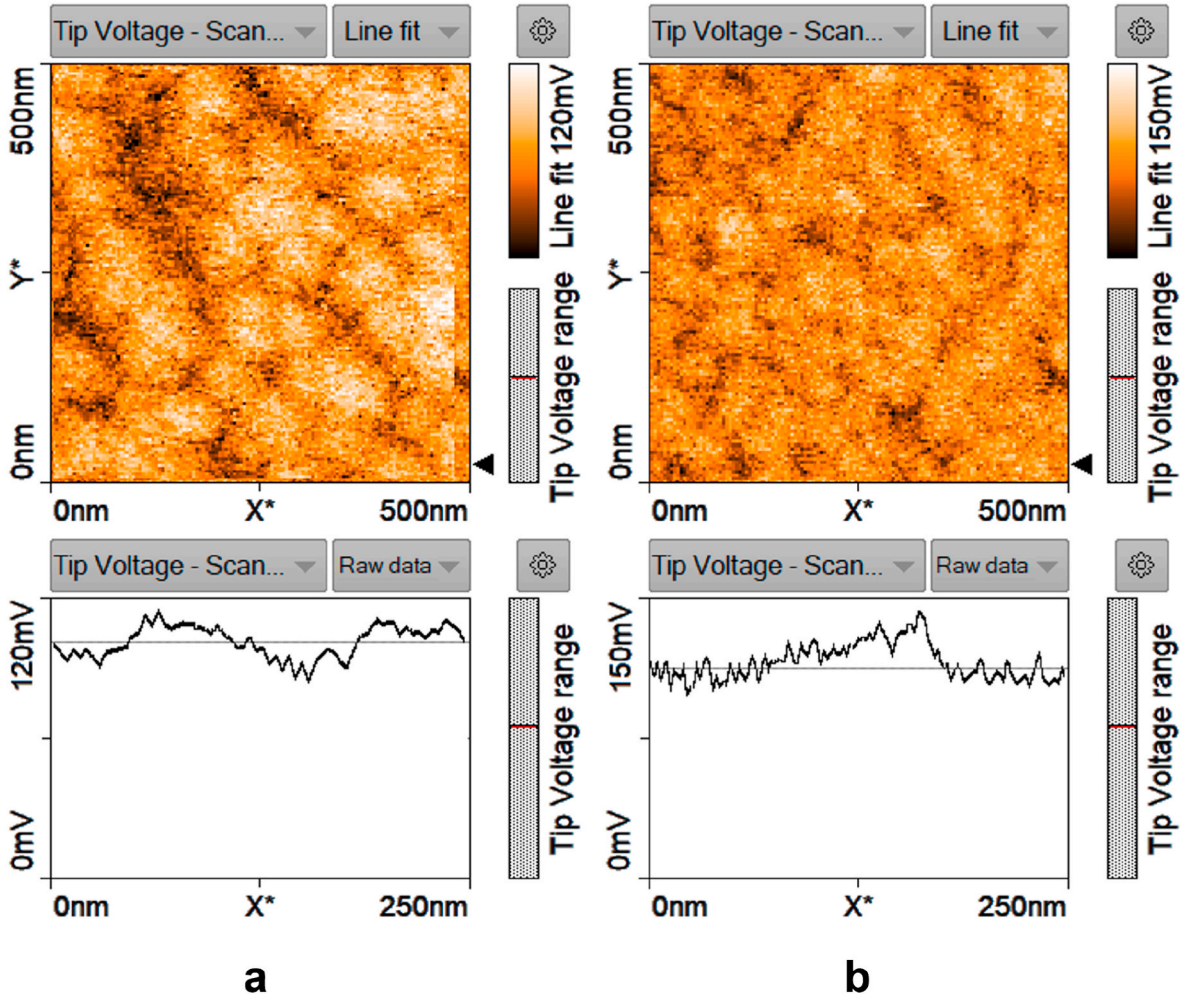

Fig. 8. KPFM surface potential map images (area of 500 × 500 nm^2) and within horizontal voltage profiles (250 nm of scan length).

Specifically, the contact surface potential values obtained by KPFM were (109 ± 10) mV for the RT-AlN thin film and (112 ± 6) mV for AlN_150 sample, in good accordance with the values achieved with no-standard procedure. These values were obtained by Nanosurf CoreAFM software, which calculates the average surface potential over the entire investigated area from the horizontal tip voltage profiles.

The procedure proposed in this paper represents an interesting potentiality to evaluate the surface potential in a broader interval of AC amplitude.

5. Conclusions

In summary, this work shows a PFM-based methodology applied on ceramic piezoelectric films for evaluating the proper piezoelectric coefficient by minimizing the electrostatic contribution that generally affects and distorts the measurement. Sputtered aluminum nitride thin films grown at different substrate temperatures were characterized. The method consists in sweeping the DC voltage applied to the AFM tip under a fixed AC field for the evaluation of the contact surface potential difference V_{CPD} between the tip and the investigated sample. The obtained V_{CPD} values were used to correct the piezoelectric coefficient $d_{33,eff}$ from the electrostatic interactions. Kelvin Probe Force Microscopy was employed as reference standard technique to measure the surface potential confirming the reliability of the proposed experimental procedure. We consider the shown methodology of great importance. On one hand, it is possible to make reliable piezoelectric measurements by evaluating the surface potential without using the KPFM technique (thus overcoming its limitations and problems). On the other hand, the measurement of the surface potential of a material and the capability to tune it in a wide range, by applying an external field, open new perspectives for the design of innovative devices, especially in the field of biomaterials integration, since it influences bioprocesses such as cells proliferation, differentiation, attachment, and adhesion on the films surface.

CRediT authorship contribution statement

M.A. Signore: Writing – original draft, Validation, Supervision, Methodology, Investigation, Formal analysis, Data curation, Conceptualization. **L. Francioso:** Validation, Supervision, Methodology, Data curation, Conceptualization. **C. De Pascali:** Visualization, Validation, Software, Data curation. **A. Serra:** Validation, Methodology, Investigation, Data curation. **D. Manno:** Validation, Methodology, Formal analysis, Data curation. **G. Rescio:** Methodology, Data curation. **F. Quaranta:** Validation, Investigation. **E. Melissano:** Investigation, Data curation. **L. Velardi:** Writing – original draft, Visualization, Validation, Methodology, Investigation, Data curation, Conceptualization.

Declaration of competing interest

The authors declare that they ave no known competing financial interests or personal relationships that could have appeared to influence the work reported in this paper.

Data availability

No data was used for the research described in the article.

References

[1] J. Chen, K. Xu, Applications of atomic force microscopy in materials, semiconductors, polymers, and medicine: a minireview, Instrum. Sci. Technol. 48 (2020) 667, https://doi.org/10.1080/10739149.2020.1764030.

[2] S. Wu, Q. Liu, Z. Wang, Z. Zhang, Z. Lu, R. Xiong, J. Yao, D. Wang, Effects of low voltage ionized hydrogen ion bombardment in semi-insulating GaAs, Vacuum 215 (2023), 112314, https://doi.org/10.1016/j.vacuum.2023.112314.

[3] P. Sriboriboon, H. Qiao, O. Kwon, et al., Deep learning for exploring ultra-thin ferroelectrics with highly improved sensitivity of piezoresponse force microscopy, npj Comput. Mater. 9 (2023) 28, https://doi.org/10.1038/s41524-023-00982-0.

[4] Y. Zhang, J. Zuo, P. Li, Y. Gao, W. He, Z. Zheng, Study of the nanoscale electrical performance of NiO thin films by C-AFM and KPFM techniques: the effect of grain boundary barrier, Phys. E Low-dimens. Syst. Nanostruct. 111 (2019) 75–78, https://doi.org/10.1016/j.physe.2019.03.005.

[5] Z. Li, L. Li, G. Zhang, L. Song, Z. Tu, C. Han, AZO work function enhanced by oxygen plasma immersion ion implantation, Vacuum 212 (2023), 112038, https://doi.org/10.1016/j.vacuum.2023.112038.

[6] S. Guchhait, A. Ahmad, H. Aireddy, A.K. Das, The study of converse piezoelectric-effect of ZnO thin film, AIP Conf. Proc. 2142 (2019), 080010, https://doi.org/10.1063/1.5122438.

[7] Q.N. Chen, Y. Ou, F.Y. Ma, J.Y. Li, Mechanisms of electromechanical coupling in strain-based scanning probe microscopy, Appl. Phys. Lett. 104 (2014), 242907, https://doi.org/10.1063/1.4884422.

[8] Daehee Seol, Seunghun Kang, Changhyo Sun, Yunseok Kim, Significance of electrostatic interactions due to surface potential in piezoresponse force microscopy, Ultramicroscopy 207 (2019), 112839, https://doi.org/10.1016/j.ultramic.2019.112839.

[9] S. Kim, D. Seol, X.L. Lu, M. Alexe, Y. Kim, Electrostatic-free piezoresponse force microscopy, Sci. Rep. 7 (2017), 41657, https://doi.org/10.1038/srep41657.

[10] Daehee Seol, Seunghun Kang, Changhyo Sun, Yunseok Kim, Significance of electrostatic interactions due to surface potential in piezoresponse force microscopy, Ultramicroscopy 207 (2019), 112839, https://doi.org/10.1016/j.ultramic.2019.112839.

[11] N. Balke, S. Jesse, Q. Li, P. Maksymovych, M.B. Okatan, E. Strelcov, A. Tselev, S. V. Kalinin, Current and surface charge modified hysteresis loops in ferroelectric thin films, J. Appl. Phys. 118 (2015), 072013, https://doi.org/10.1063/1.4927811.

[12] B.J. Rodriguez, C. Callahan, S.V. Kalinin, R. Proksch, Dual-frequency resonance-tracking atomic force microscopy, Nanotechnology 18 (2007), 475504, https://doi.org/10.1088/0957-4484/18/47/475504.

[13] N.C. Miller, H.M. Grimm, W.S. Horne, G.R. Hutchison, Accurate electromechanical characterization of soft molecular monolayers using piezo force microscopy, Nanoscale Adv. 1 (2019) 4834, https://doi.org/10.1039/C9NA00638A.

[14] R. Berger, Kelvin probe force microscopy: from single charge detection to device characterization, Microsc. Microanal. 25 (2019) 1509, https://doi.org/10.1017/S1431927619015083.

[15] W. Melitz, J. Shen, A.C. Kummel, S. Lee, Kelvin probe force microscopy and its application, Surf. Sci. Rep. 66 (2011) 1–27, https://doi.org/10.1016/j.surfrep.2010.10.001.

[16] R. Izumi, Y.J. Li, Y. Naitoh, Y. Sugawara, Study of high–low KPFM on a pn-patterned Si surface, Microscopy 71 (2022) 98–103, https://doi.org/10.1093/jmicro/dfab055.

[17] J.I. Kilpatrick, E. Kargin, B.J. Rodriguez, Comparing the performance of single and multifrequency Kelvin probe force microscopy techniques in air and water, Beilstein J. Nanotechnol. 13 (2022) 922–943, https://doi.org/10.3762/bjnano.13.82.

[18] J. Xu, D. Chen, Interpreting Kelvin probe force microscopy on semiconductors by Fourier analysis, J. Appl. Phys. 129 (2021), 034301, https://doi.org/10.1063/5.0024073.

[19] S. Chen, H. Dong, J. Yang, Surface potential/charge sensing techniques and applications, Sensors 20 (2020) 1690, https://doi.org/10.3390/s20061690.

[20] W. Fu, L. Jiang, E.P. van Geest, L.M.C. Lima, G.F. Schneider, Sensing at the surface of graphene field-effect transistors, Adv. Mater. 29 (2016), 1603610, https://doi.org/10.1002/adma.201603610.

[21] B.M. Lowe, C.K. Skylaris, N.G. Green, Y. Shibuta, T. Sakata, Calculation of surface potentials at the silica–water interface using molecular dynamics: challenges and opportunities, Jpn. J. Appl. Phys. 57 (2018), 04FM02, https://doi.org/10.7567/JJAP.57.04FM02.

[22] P. Salvo, B. Melai, N. Calisi, C. Paoletti, F.G. Bellagambi, A. Kirchhain, M. Trivella, R. Fuoco, F. Di Francesco, Graphene-based devices for measuring pH, Sensor. Actuator. B Chem. 256 (2018) 976–991, https://doi.org/10.1016/j.snb.2017.10.037.

[23] J. Wang, Y. Chen, Y. Wang, Y. Xu, Z. Zhang, Computational study of surface orientation effect of wurtzite GaN on CH4 and CO sensing mechanism, Vacuum 208 (2023), 111724, https://doi.org/10.1016/j.vacuum.2022.111724.

[24] X. Duan, Y. Li, N.K. Rajan, D.A. Routenberg, Y. Modis, M. Reed, Quantification of the affinities and kinetics of protein interactions using silicon nanowire biosensors, Nat. Nanotechnol. 7 (2012) 401–407, 10.1038%2Fnnano.2012.82.

[25] E.O. Carvalho, M.M. Fernandes, J. Padrao, A. Nicolau, J. Marqués-Marchán, A. Asenjo, F.M. Gama, C. Ribeiro, S. Lanceros-Mendez, Tailoring bacteria response by piezoelectric stimulation, ACS Appl. Mater. Interfaces 11 (2019) 27297–27305, https://doi.org/10.1021/acsami.9b05013.

[26] F.J. Nordt, Alterations in surface charge density versus changes in surface charge topography in aging red blood cells, Blut 40 (1980) 233–238, https://doi.org/10.1007/BF01080182.

[27] K. Madhu, S. Kannan, A. Perumal, P. Shanmugam, Biofunctionalized nanocomposite coating on Cp-titanium with reduce implant failures, Vacuum 215 (2023), 112328, https://doi.org/10.1016/j.vacuum.2023.112328.

[28] F. Chen, H. Huang, L. Guo, Y. Zhang, T. Ma, The role of polarization in photocatalysis, Angew. Chem. Int. Ed. 58 (2019) 10061–10073, https://doi.org/10.1002/anie.201901361.

[29] X. Zhu, T.G. Mason, Separating nanoparticles by surface charge group using pH-controlled passivated gel electrophoresis, Soft Mater. 14 (2016) 204–209, https://doi.org/10.1080/1539445X.2016.1183675.
[30] S. Metwally, U. Stachewicz, Surface potential and charges impact on cell responses on biomaterials interfaces for medical applications, Mater. Sci. Eng. C 104 (2019), 109883, https://doi.org/10.1016/j.msec.2019.109883.
[31] M. Li, X. Chu, D. Wang, L. Jian, L. Liu, M. Yao, D. Zhang, Y. Zheng, X. Liu, Y. Zhang, F. Peng, Tuning the surface potential to reprogram immune microenvironment for bone regeneration, Biomaterials 282 (2022), 121408, https://doi.org/10.1016/j.biomaterials.2022.121408.
[32] B.L. Tang, B. Zhang, J.J. Zhuang, Q. Wang, L.Q. Dong, K. Cheng, W. Weng, Surface potential-governed cellular osteogenic differentiation on ferroelectric polyvinylidene fluoride trifluoroethylene films, Acta Biomater. 74 (2018) 291–301, https://doi.org/10.1016/j.actbio.2018.04.051.
[33] N.A. kamel, Bio-piezoelectricity: fundamentals and applications in tissue engineering and regenerative medicine, Biophys. Rev. 14 (2022) 717–733, 10.1007%2Fs12551-022-00969-z.
[34] H. Zhao, C. Liu, Y. Liu, Q. Ding, T. Wang, H. Li, H. Wu, T. Ma, Harnessing electromagnetic fields to assist bone tissue engineering, Stem Cell Res. Ther. 14 (2023) 7, https://doi.org/10.1186/s13287-022-03217-z.
[35] E. Soergel, Piezoresponse force microscopy (PFM), J. Phys. D Appl. Phys. 44 (2011), 464003, https://doi.org/10.1088/0022-3727/44/46/464003.
[36] N. Tranvouez, P. Steyer, A. Malchère, P. Boulet, F. Capon, J.P. Bauer, J.F. Pierson, Effect of thermal stresses formed during air annealing of amorphous lanthanum cuprate thin films deposited on silicon substrate, Coatings 10 (2020) 613, https://doi.org/10.3390/coatings10070613.
[37] V. Chawla, R. Jayaganthan, A.K. Chawla, R. Chandra, Microstructural characterizations of magnetron sputtered Ti films on glass substrate, J. Mater. Process. Technol. 209 (2009) 3444–3451, https://doi.org/10.1016/j.jmatprotec.2008.08.004.
[38] I.H. Mejri, K. Omri, I. Ghilouf, J.P.B. Silva, M.J.M. Gomes, L. El Mir, Resistive switching behavior in ZnO:Ca thin films deposited by a pulsed laser deposition technique, Appl. Phys. A 129 (2023) 210, https://doi.org/10.1007/s00339-023-06508-1.
[39] A. le Febvrier, N. Tureson, N. Stilkerich, G. Greczynski, Per Eklund, Effect of impurities on morphology, growth mode, and thermoelectric properties of (111) and (001) epitaxial-like ScN films, J. Phys. D Appl. Phys. 52 (2019), 035302, https://doi.org/10.1088/1361-6463/aaeb1b.
[40] L. Calcagnile, G. Quarta, M. D'Elia, D. Muscogiuri, L. Maruccio, K. Butalag, G. Gianfrate, C. Sanapo, U. Toma, Instrumental developments at the IBA-AMS dating facility at the University of Lecce, Nucl. Instrum. Methods Phys. Res. Sect. B Beam Interact. Mater. Atoms 240 (2005) 22, https://doi.org/10.1016/j.nimb.2005.06.081.
[41] N. Balke, S. Jesse, P. Yu, B. Carmichael, S.V. Kalinin, A. Tselev, Quantification of surface displacements and electromechanical phenomena via dynamic atomic force microscopy, Nanotechnology 27 (2016), 425707, https://doi.org/10.1088/0957-4484/27/42/425707.
[42] Y.C. Huang, T.C. Hsieh, T.J. Hong, C.H. Wu, Y.T. Ho, Y.W. Tsai, J.M. Lin, H.L. Kao, S.J. Chang, The ultra-thin AlN epitaxy on monolayer WS2 by helicon sputtering at 400 ∘C, Vacuum 207 (2023), 111681, https://doi.org/10.1016/j.vacuum.2022.111681.
[43] L. Polak, R.J. Wijngaarden, Two competing interpretations of Kelvin probe force microscopy on semiconductors put to test, Phys. Rev. B 93 (2016), 195320, https://doi.org/10.1103/PhysRevB.93.195320.
[44] N.Q. Khanh, J. Radó, Z.E. Horváth, et al., The effect of substrate bias on the piezoelectric properties of pulse DC magnetron sputtered AlN thin films, J. Mater. Sci. Mater. Electron. 31 (2020) 22833–22843, https://doi.org/10.1007/s10854-020-04810-9.
[45] F. Martin, P. Muralt, M.-A. Dubois, A. Pezous, Thickness dependence of the properties of highly c-axis textured AlN thin films, J. Vac. Sci. Technol. A 22 (2004) 361–365, https://doi.org/10.1116/1.1649343.
[46] M. Reusch, K. Holc, W. Pletschen, L. Kirste, A. Žukauskaite, T. Yoshikawa, D. Iankov, O. Ambacher, V. Lebedev, Analysis and optimization of sputter deposited AlN-layers for flexural plate wave devices, J. Vac. Sci. Technol. B 34 (2016), 052001, https://doi.org/10.1116/1.49595800.